Spatially-resolved in-situ quantification of biofouling using optical coherence tomography (OCT) and 3D image analysis in a spacer filled channel

Fortunato, Luca; Bucs, Szilárd; Linares, Rodrigo Valladares; Cali, Corrado; Vrouwenvelder, Johannes S.; Leiknes, Tor Ove

DOI
10.1016/j.memsci.2016.11.052

Publication date
2017

Document Version
Final published version

Published in
Journal of Membrane Science

Journal of Membrane Science 524 (2017) 673–681

Contents lists available at ScienceDirect

Journal of Membrane Science

journal homepage: www.elsevier.com/locate/memsci

Spatially-resolved *in-situ* quantification of biofouling using optical coherence tomography (OCT) and 3D image analysis in a spacer filled channel

Luca Fortunato[a,*], Szilárd Bucs[a], Rodrigo Valladares Linares[a], Corrado Cali[b], Johannes S. Vrouwenvelder[a,c,d], TorOve Leiknes[a]

[a] *King Abdullah University of Science and Technology (KAUST), Water Desalination and Reuse Center (WDRC), Biological and Environmental Science & Engineering (BESE), Thuwal 23955-6900, Saudi Arabia*

[b] *King Abdullah University of Science and Technology (KAUST), Division of Biological and Environmental Science and EngineeringThuwal 23955-6900, Saudi Arabia*

[c] *Department of Biotechnology, Faculty of Applied Sciences, Delft University of Technology, Van der Maasweg 9, 2629 HZ Delft, The Netherlands*

[d] *Wetsus, European Centre of Excellence for Sustainable Water Technology, Oostergoweg 9, 8911 MA Leeuwarden, The Netherlands*

ARTICLE INFO

Keywords:
OCT
Feed spacer
Fouling
Ultrafiltration
Biofilm

ABSTRACT

The use of optical coherence tomography (OCT) to investigate biomass in membrane systems has increased with time. OCT is able to characterize the biomass *in-situ* and non-destructively. In this study, a novel approach to process three-dimensional (3D) OCT scans is proposed. The approach allows obtaining spatially-resolved detailed structural biomass information. The 3D biomass reconstruction enables analysis of the biomass only, obtained by subtracting the time zero scan to all images. A 3D time series analysis of biomass development in a spacer filled channel under representative conditions (cross flow velocity) for a spiral wound membrane element was performed. The flow cell was operated for five days with monitoring of ultrafiltration membrane performance: feed channel pressure drop and permeate flux. The biomass development in the flow cell was detected by OCT before a performance decline was observed. Feed channel pressure drop continuously increased with increasing biomass volume, while flux decline was mainly affected in the initial phase of biomass accumulation.

The novel OCT imaging approach enabled the assessment of spatial biomass distribution in the flow cell, discriminating the total biomass volume between the membrane, feed spacer and glass window. Biomass accumulation was stronger on the feed spacer during the early stage of biofouling, impacting the feed channel pressure drop stronger than permeate flux.

1. Introduction

In the last decades the use of membrane filtration to produce high quality drinking water has increased. One of the major problem of membrane filtration systems is biofouling [1,2]. Biofilm formation is caused by the accumulation of microorganisms, including extracellular polymeric substances (EPS) produced by microorganisms, on a surface due to either deposition and/or growth. A biofilm causing an unacceptable decline in membrane performance is defined as biofouling. Performance losses are caused by increase in feed channel pressure drop, permeate flux reduction and/or salt passage [3].

The complex configuration of the membrane modules makes it difficult to study biofouling *in-situ*. Lab-scale monitors have been developed to allow easier access and better analyses of biofilm development in spiral wound membrane modules [4,5]. Membrane fouling simulator (MFS) was proved to be a suitable tool to study biofouling in spiral wound membrane systems [6].

A key aspect of biomass studies involves the analysis of biomass structure [7], which can predict the biomass behavior, and thus, the impact on membrane filtration performance. Several approaches are reported in literature to study biomass, most often involving destructive methods [8,9]. Microscopic techniques are considered an important tool for biomass structure investigation. However, these techniques involve sample preparation, and are less suitable to study the

* Correspondence to: King Abdullah University of Science and Technology (KAUST), Water Desalination and Reuse Center (WDRC), Division of Biological and Environmental Science and Engineering (BESE), Al-Jazri Bldg, Thuwal 23955-6900, Saudi Arabia.

E-mail addresses: Luca.Fortunato@kaust.edu.sa (L. Fortunato), Szilard.Bucs@kaust.edu.sa (S. Bucs), Rodrigo.Valladares@kaust.edu.sa (R.V. Linares), Johannes.Vrouwenvelder@kaust.edu.sa, J.S.Vrouwenvelder@tudelft.nlHans.Vrouwenvelder@wetsus.nl (J.S. Vrouwenvelder), Torove.Leiknes@kaust.edu.sa (T. Leiknes).

http://dx.doi.org/10.1016/j.memsci.2016.11.052
Received 5 July 2016; Received in revised form 23 October 2016; Accepted 20 November 2016
Available online 21 November 2016
0376-7388/

biomass development *in-situ*.

To better understand the biomass development in membrane systems, *in-situ* qualitative and quantitative analyses of the biomass under operational conditions are needed. Several techniques are currently available to study the biomass formation under membrane operational conditions, such as nuclear magnetic resonance spectroscopy (NMR), planar optodes and optical coherence tomography (OCT) [10].

Optical coherence tomography (OCT) has the ability to investigate biomass formation and 3D structure *in-situ,* without any staining procedures, OCT has recently been used to study biofouling in membrane filtration systems [11,12]. OCT was used to characterize the biofilm deposited on the membrane [13,14]. Dreszer et al. [15] evaluated the suitability of OCT to study the biofilm development, and permeate flux change using microfiltration (MF) membrane. The biofilm time-resolved deformation was calculated in real-time from cross sectional OCT scans [16]. Fortunato et al. [17] monitored in real-time the fouling layer evolution in a submerged membrane bioreactor. Yang et al. [18] demonstrated the importance of 3D structural analyses for biofilms grown on a membrane surface. West et al. [19] correlated the biomass accumulation to the feed channel pressure drop increase in time using OCT. Li et al. [20] used the 3D OCT to characterize the biofilm developed on carriers in lab-scale moving bed biofilm reactors. The 3D image analysis offers several advantages with respect to the 2D analysis, such as quantification of biomass growth defined by biovolume, porosity, heterogeneity, thickness and spatial distribution.

The objective of this study was to spatially-resolve quantifying the biomass formation in a spacer filled flow channel under representative conditions for spiral wound membrane filtration systems. A novel approach is proposed to process 3D OCT scans to quantify biomass distribution over the feed spacer and membrane surfaces and to evaluate the impact of accumulated biomass on membrane filtration performance measured by feed channel pressure drop and permeate flux.

2. Materials and methods

Biomass formation with OCT was studied in a spacer filled channel under representative operating conditions for spiral wound membrane systems.

2.1. Experimental setup

For all the experiments the biomass was grown on sheet of membrane and spacer in membrane fouling simulator (MFS) [21]. To enable *in-situ* non-destructive observation of the biomass formation by OCT, the MFS cover contained five millimeter thick glass window. For each experiment a 20 cm×10 cm ultrafiltration (PAN UF, with a molecular cut-off of 150 kDa) membrane coupon and 31 mil (787 μm, Trisep, USA) thick feed spacer was inserted into the MFS. The ultrafiltration (UF) membrane was necessary to allow water permeation at one bar through the membrane due to the low hydraulic pressure thereby mimicking the flux through the system and resulting hydraulic resistance. Moreover, the use of this membrane enabled the investigation of the biofouling in spacer filled channel without any influence of concentration polarization or other types of fouling.

The MFS was operated under constant hydraulic pressure of one bar at ambient temperature (20°C). The MFS was fed with tap water by a gear pump (Cole Palmer, USA) at a flow rate of 45.5 L h^{-1}, resulting in a 0.16 m s^{-1} linear flow velocity at the inlet side of the flow channel, representative for practice [22]. The tap water was filtered through carbon and cartridge filters (5 μm pore size) to remove residual chlorine and to avoid larger particles entering the MFS (Fig. 1). Water permeation though the UF membrane was accomplished with one bar pressure. The hydraulic pressure was regulated by a back-pressure valve (Hydra cell, Wanner Engineering Inc., USA) located on the outflow of the MFS. During the five days experimental period the biomass development was monitored by OCT imaging and its impact on performance was evaluated by the feed channel pressure drop (Deltabar, Endress+Hauser PMD75, Germany) [23,27], and permeate flux (Sensirion, Switzerland) measurements.

2.2. Biomass growth

To enhance biomass formation a nutrient solution containing sodium acetate, sodium nitrate, and sodium phosphate in a ratio of 100:20:10 was dosed to the feed water. A concentrated nutrient solution was prepared and continuously dosed (Stepdos 03, KNF Lab, Germany) into the feed stream of the MFS at a flow rate of 1 ml min^{-1}, resulting in 800 μg C L^{-1} carbon concentration in the MFS feed water. To avoid bacterial growth in the nutrient stock the pH of the solution was adjusted to 11, with sodium hydroxide (1 M).

The setup was operated for 24 h with tap water only to condition the membrane before starting nutrient dosage. During the first hours of the biofouling experiments the setup showed constant water permeation (Fig. 1).

2.3. Imaging and data processing

An OCT (Thorlabs GANYMEDE GmbH, Dachau, Germany) with a central wavelength of 930 nm equipped with a 5× telecentric scan lens (Thorlabs LSM 03BB) was used to investigate the biomass growth in the MFS flow channel containing membrane and feed spacer sheets. The MFS was mounted on a stage under the OCT probe in order to monitor the biomass development over time in a fixed area (one feed spacer square element) positioned at 5 cm from the feed inlet over time (Fig. 2). The monitored area corresponds to 5.3 mm×5.3 mm with 2.7 μm axial resolution. The OCT lens depth of field was adjusted to 950 μm (slightly higher than the total flow channel height of 787 μm) to allow capturing a part of the membrane and cover glass window. The resulting image stack resolution was (545×545×482) pixels, with a lateral resolution of 11 μm.

The OCT images were processed using ImageJ software (Version 1.48). A multi-step processing sequence was applied, consisting of (1) subtraction the initial image t_0 from the image taken at any given time (t_X), (2) adjustment of contrast and brightness of the resulting image (3) application of a median filter and (4) binarization of the image with Otsu algorithms [24]. This approach allows the elimination of the cover glass, membrane and feed spacer from the OCT image stack, and allowing the quantification of the accumulated biomass (Fig. 3).

The initial scan was subtracted from the successive scans (step 1) in order to avoid the over or the under estimation of the accumulated biomass in the scanned area, the feed spacer geometry and other structures present in the flow channel needed to be eliminated from the scans. The binarized datasets were then further analyzed to assess the accumulated biomass volume (V_{Tot}) using the ImageJ plug-in voxel counter.

Two different biomass descriptors were used to quantify the biomass development in the flow channel. The total biovolume (mm^3/cm^2) for the scanned (monitored) area was calculated with the following equation:

$$V_{Scanned} = \frac{V_{Tot}}{A_{Scanned}} \quad (1)$$

where V_{Tot} is the total biomass volume and $A_{Scanned}$ is the scanned area (in this case 0.53 cm×0.53 cm). The specific biovolume ($V_{Specific}$) was calculated using the following equation:

$$V_{Specific} = \frac{\sum V^i_{biomass}}{\sum A^i} = \frac{V_{Tot}}{\sum A^i} \quad (2)$$

where $V_{biomass}$ is the biomass volume, A^i the covered area of the

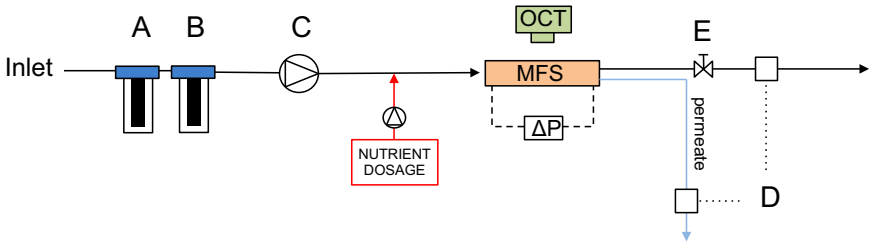

Fig. 1. Schematic representation of the experimental setup consisting of carbon (A) and cartridge filters (B), a tank containing nutrient solution, pump (C), dosing pump, flow meter (D), pressure reducing valve (E), differential pressure transmitter, membrane fouling simulator (MFS), and optical coherence tomography (OCT) device.

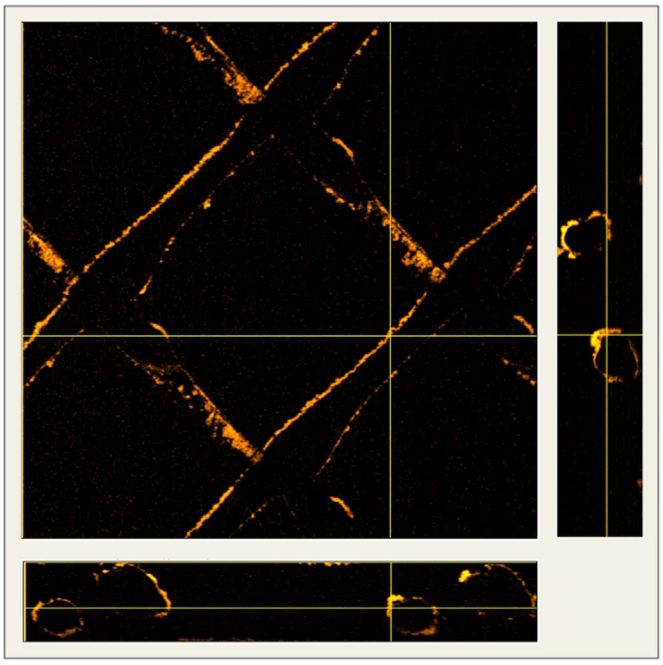

Fig. 2. Orthogonal view of OCT images of accumulated biomass (orange color) on the feed spacer, membrane and cover glass window (5.3 mm×5.3 mm×0.95 mm) in the MFS after one day of operation. The yellow lines shows the location of the orthoslices. (For interpretation of the references to color in this figure legend, the reader is referred to the web version of this article.)

investigated element (i) of the flow channel (membrane, feed spacer, cover glass). The total biomass V_{Tot} is the sum of biomass accumulated on the membrane, spacer and cover glass surface. The specific biovolume ($V^i_{Specific}$) for each element was calculated using the following equation:

$$V^i{}_{Specific} = \frac{V^i_{biomass}}{A^i} \quad (3)$$

where $V^i_{Specific}$ is the specific biovolume of each individual flow cell element (*i.e.* membrane, feed spacer, cover glass). The developed approach allows to separately evaluate the accumulated biomass on the membrane, feed spacer and cover glass surface respectively.

Three different masks (A, B, C) were created for the three elements one for the spacer (B) and two for the glass (A) and membranes (C) (supplementary material Fig. S1). The size of masks was determined according to the maximum thickness of the biomass observed on the surface of the elements. For the cases where the biomass is attached simultaneously to two elements (supplementary material Fig. S2), the biomass volume is calculated by equally distributing the biomass over the two elements. First the voxels are counted in the areas where the masks belonging to two different elements intersect (A∩B and B∩C) and the total number of voxel are divided by two and subtracted from the total number of voxels counted in each mask (supplementary material equations S1 – S8).

3. Results

In this study, the biomass development in a spacer filled channel was monitored *in-situ* non-destructively with OCT (optical coherent tomography). A novel approach was used to process the 3D OCT scans

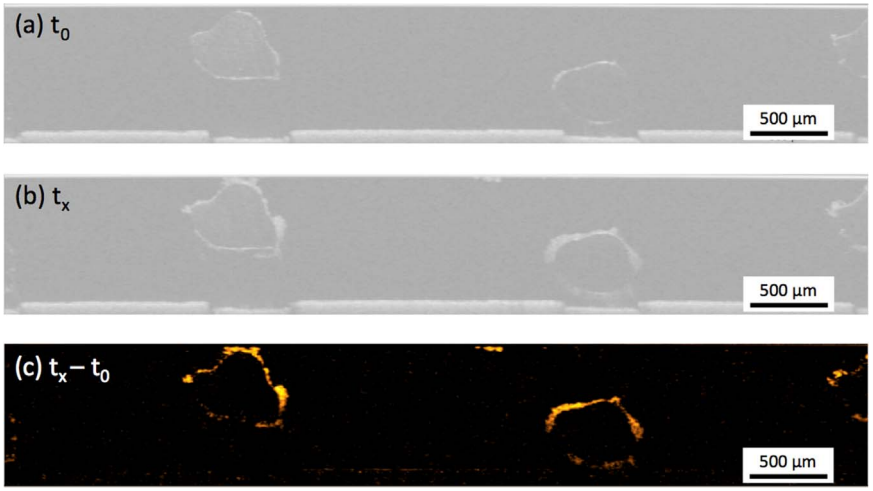

Fig. 3. OCT scans at different times at the same position: (a) image before biomass formation at t_0, (b) image with accumulated biomass after certain time period t_X and spatially-resolved biomass quantification (c) after subtracting the image at time 0 from the image taken after a certain time period (t_X–t_0). The final image shows only the biomass (orange color) without the background signals (glass, membrane and feed spacer). (For interpretation of the references to color in this figure legend, the reader is referred to the web version of this article.)

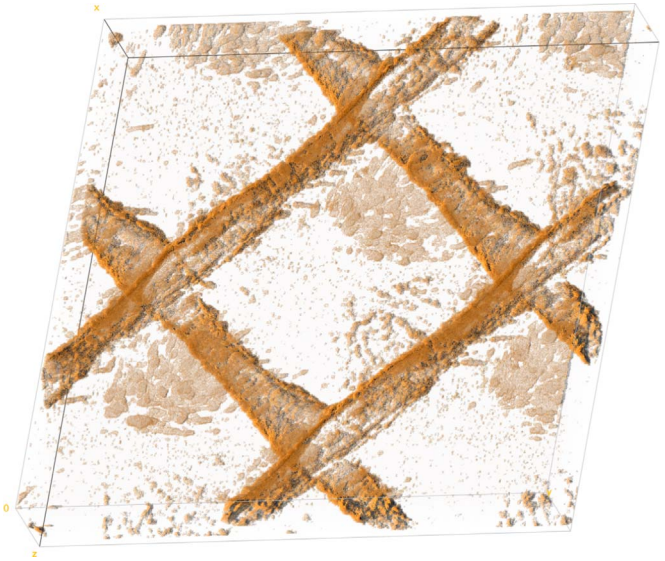

Fig. 4. Three-dimensional (3D) rendered OCT image with biomass (brown color), the spacer, membrane and cover glass were eliminated by using the scan at time zero as baseline. (For interpretation of the references to color in this figure legend, the reader is referred to the web version of this article.)

allowing spatially resolved (i) biomass volume measurements in time, and (ii) biomass distribution quantification and visualization. Membrane performance parameters, such as pressure drop and permeate flux, were monitored during the study.

3.1. Image processing

The OCT was used to monitor the biomass formation at a fixed position in the spacer filled channel two times per day throughout the five days experimental period. To quantify the biomass development the accumulated biomass volume was calculated from the OCT scans. The feed spacer was not transparent for the OCT. When the feed spacer was present a shift of the location of the membrane and possible biomass below the feed spacer filaments were observed (Fig. 3a,b). The applied image processing method allows visualization of the biomass only and thus excludes the membrane, feed spacer and cover glass structure from the collected scans (Fig. 4).

The rendered volume development over time shown in Fig. 5 represents only the biomass.

3.2. Biomass quantification

OCT scans confirmed the presence of biomass after one day of operation with nutrient dosage (Fig. 6a). As reported in Section 2.3, the biomass grown in a specific area can be quantified with different descriptors as biomass volume (V_{tot}), scanned biovolume (V) and specific biovolume ($V_{Specific}$). The scanned biovolume normalizes the biomass volume for the scanned area, allowing comparison of data obtained with the same feed spacer (and flow channel height). However, the specific biovolume is the only descriptor that allows comparing the biomass volume with different feed spacers, normalizing the biomass volume for the available surfaces (membrane, feed spacer and glass window) in the flow cell. In Table 1 are reported the biomass values over the time according to different descriptors.

The OCT scans taken periodically during the experimental period confirm the exponential biomass growth (r^2=0.97). In the first two days of nutrient dosage only a small amount of biomass was detected. A specific biovolume of 0.22 $mm^3\,cm^{-2}$ was detected in the position monitored after one day, corresponding to 0.9% of the available volume. From the third day a steep increase in biomass volume was observed (Fig. 6a). Towards the end of the study the rate of increase in biomass volume started to decrease. At the end of the experimental period, the final biomass volume occupied 24.9% of the monitored area reaching a specific biovolume of 6.29 $mm^3\,cm^{-2}$.

3.3. Membrane performance

Pressure drop over the feed channel and permeate flux through the membrane were monitored throughout the experimental period. Additionally, biomass volume was calculated from the OCT scans.

Biomass accumulation was confirmed by the feed channel pressure drop increase. A rapid increase in feed channel pressure drop was observed after two days of operation with nutrient dosage (Fig. 6b). By the end of the experimental period the normalized feed channel pressure drop reached a value of 980 mbar/m due to biomass accumulation.

Feed channel pressure drop was measured over the whole flow channel length (20 cm) while the OCT data is from a fixed position. In the present study, the OCT scans covered a much smaller area than pressure drop measurements, 5.3 mm×5.3 mm in our case with a 2.7 μm resolution positioned at 5 cm from the feed inlet. This gives the possibility to detect biomass deposition and growth at an early stage with micrometers resolution.

Because of the use of a UF membrane, the initial permeate flux of the clean membrane was 105 $L\,m^{-2}\,h^{-1}$. With nutrient dosage a small flux decline was observed at the first day of the experimental period, followed by a rapid decrease (1.27 $L\,m^{-2}\,h^{-1}$) on the second and third days (Fig. 6c). On the fourth day the rate of flux decline was slowed down (0.21 $L\,m^{-2}\,h^{-1}$) and reached a final permeate flux of 30 $L\,m^{-2}\,h^{-1}$ at the end of the experimental period.

3.4. Biomass distribution

Images presented in Fig. 5 show the biomass distribution in the flow channel with time. On the first day of MFS operation with nutrient dosage, biomass accumulation was mainly observed through the OCT on the feed spacer. From the second day on, biomass was seen to accumulate as well on the membrane and glass surfaces.

The method adopted in this experiment allows studying and evaluating the distribution of the biomass on the different elements of the flow channel (*i.e.* membrane, cover glass, feed spacer). The total biomass volume of the monitored area was further analyzed and the biomass volume accumulated on each element of the flow channel was calculated. Fig. 7a shows the biomass volume development for each element present in the MFS: feed spacer, cover glass, and membrane surface. For the fifth day of the experimental period, biomass volume calculation for the different elements of the flow channel was not possible due to the high amount of accumulated biomass. As the biomass develops on different locations and merged to form a continuous biomass volume makes it impossible to calculate the exact amount of biomass volume per element. The method of biomass localization is suitable for early stage when the biomass does not cover most of the available volume, which is representative of real operative conditions.

As seen in Fig. 7a, the biomass mostly attached to the feed spacer (86% of total biomass volume) after one day. As the total biomass volume increased with time, the ratio between the biomass volume on the feed spacer and total biomass volume decreased. By the second day, almost about the same biomass volume was accumulated on the feed spacer as on the membrane (58% on the feed spacer).

However, considering the different surface areas available on the membrane, feed spacer and glass windows, the volume deposited on each element can be expressed as specific biovolume for each element, defined as the biomass volume over the available surface area (see Eq. (3)). The proposed biomass descriptor allows comparing the biomass

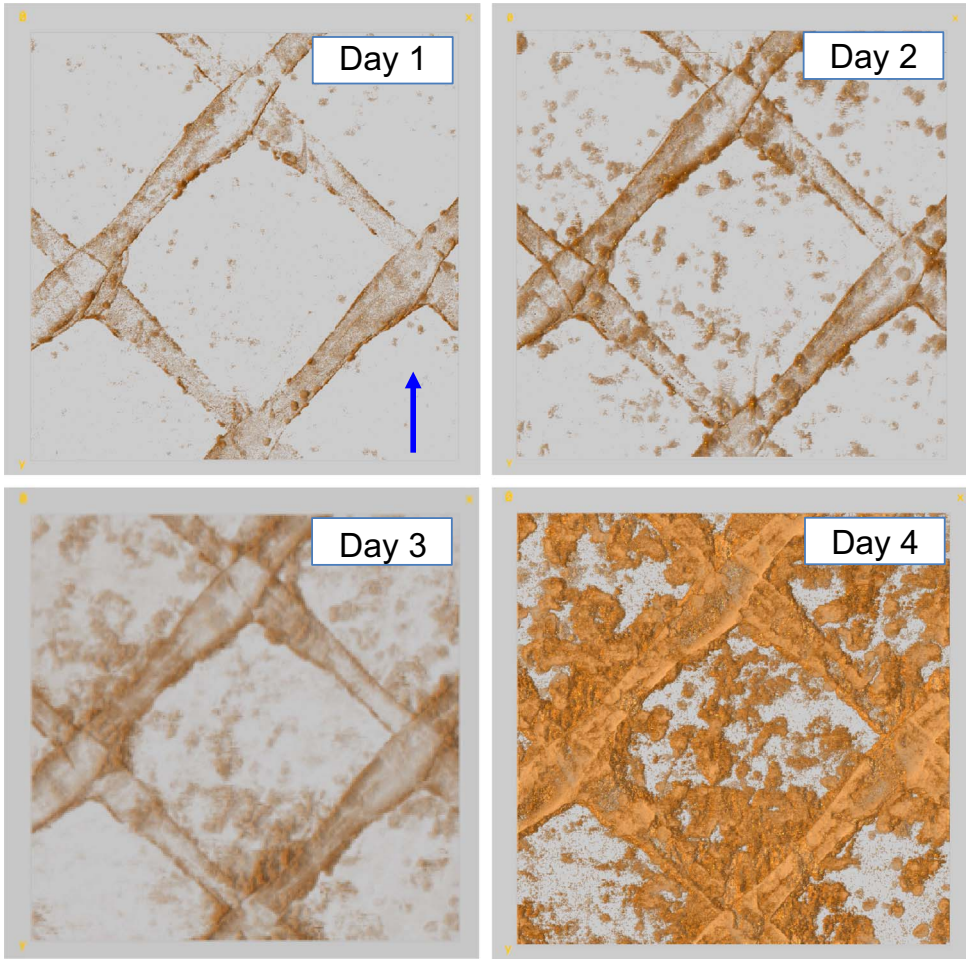

Fig. 5. Biomass development over time. Flow direction from bottom to top (arrow).

growing on different surfaces and normalizing the biomass volume for the available surface area. Based on image analysis and calculations of the clean flow channel, the surface area for the membrane and cover glass was 28.0 mm^2 and 21.9 mm^2 for the feed spacer respectively (Fig. 7b). Most of the biomass was accumulated on the feed spacer compared to the membrane and cover glass during the first three days of MFS operation (Fig. 7b).

3.5. Biomass and performance decline

Based on the OCT images, the accumulated biomass volume was calculated for each measurement time thus enabling to quantify changes in biomass volume. As the biomass volume increased the feed channel pressure drop increased (Fig. 8a) and the permeate flux decreased (Fig. 8b). The two performance indicators feed channel pressure drop and permeate flux, were seen to respond differently by the increasing biomass volume. During the biomass accumulation in the flow cell two phases were observed in the rate of permeate flux decline (a sharp decrease followed by less sharp decrease), while the feed channel pressure drop increased with increasing biomass.

Increase in the feed channel pressure drop can be explained by the biomass distribution in the flow channel (Fig. 8a). Quantification of the

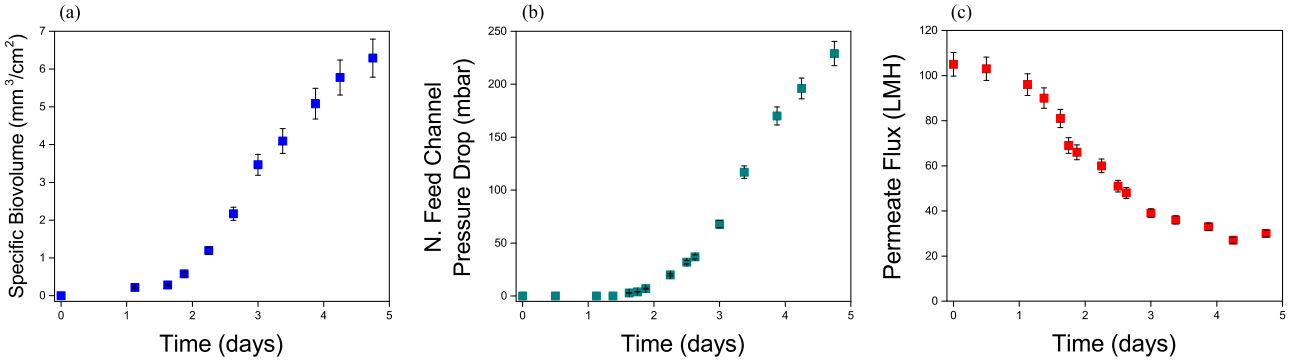

Fig. 6. Development of biomass and membrane performances over time. (a) Specific biovolume calculated from the OCT scans. (b) Normalized pressure drop over the MFS feed channel due to biomass development. (c) Permeate flux.

Table 1
Biomass development in the flow cell in time with the four descriptors.

Time (hours)	Biomass volume (mm^3)	Scanned biovolume ($mm^3\ cm^{-2}$)	Specific biovolume ($mm^3\ cm^{-2}$)	Feed channel void volume %[a]
27	0.17	0.61	0.22	0.9
39	0.22	0.78	0.28	1.1
45	0.45	1.60	0.58	2.3
54	0.93	3.31	1.19	4.7
63	1.69	6.02	2.17	8.6
72	2.7	9.61	3.47	13.7
81	3.19	11.36	4.09	16.2
93	3.96	14.10	5.08	20.1
102	4.50	16.02	5.78	22.9
114	4.90	17.44	6.29	24.9

[a] Percentage of the occupied volume occupied by the biomass from the total available volume. The fixed area=5.3 mm×5.3 mm; flow channel height=0.787 μm; feed channel volume=22.1 mm^3; feed spacer porosity =0.89; available feed channel volume=19.7 mm^3.

accumulated biomass volume on the membrane and feed spacer surfaces showed more biomass accumulation on the feed spacer than on the membrane surface (Fig. 7a).

The impact of the accumulated biomass on the different flow channel elements (membrane, feed spacer and cover glass) on the feed channel pressure drop increase is shown in Fig. 9. The biomass accumulated on the feed spacer and on the cover glass had a higher impact on the feed channel pressure drop increase than the biomass accumulated on the membrane surface.

4. Discussion

In this study a novel approach for 3D reconstruction of OCT images was presented. The method presented enables monitoring and quantification of biomass growth during operation. The approach was used to evaluate the effect of the (i) biomass on membrane performance and evaluate the (ii) biomass spatial distribution in the flow channel.

4.1. OCT image analyses

The novel image processing method presented in this study (i) eliminates the background signal (feed spacer, membrane and cover glass) from the images and (ii) enables reduction of the noise of the OCT scans. By applying the scan at time zero as a baseline, all changes in the subsequent images can be normalized to time zero. Besides subtracting the signals due to the three elements (spacer, cover glass and membrane) it removes also the signal due to the water present in the flow cell. Therefore, the proposed approach reduces the background noise, simplifies the binarization and facilitates the visualization of the biomass.

West et al. [19] used an image masking process on OCT scans to avoid the structures not corresponding to the biomass. The data presented in this study are similar with the results shown by West et al. [19], but obtained with a different OCT scan processing method. The method presented in this study enabled the detailed visualization of the biomass deposition in the monitored area.

Other imaging techniques used to study biofilms such as confocal laser scanning microscopy (CLSM) and scanning electron microscopy (SEM) generate images with a higher resolution, however, OCT enables studying larger areas necessary to gain knowledge on biofouling behavior and how it may influence the performance of membrane filtration systems. As reported by Wagner et al. [25], the structural information at micro-scale and nano-scale level might be of minor relevance to characterize the behavior of macro-scale biofilm processes as they occur in membrane filtration systems.

Meso-scale investigation of the biomass by OCT gives insight to the biofouling distribution in a spiral wound membrane module. Biomass formation under different conditions, like various spacer geometry, hydrodynamic conditions or cleaning strategies can be evaluated at a meso-scale range, due to the repetitive geometry of the feed spacer [23,26,27]. The possibility to evaluate biomass development under operational conditions, *in-situ*, at a meso-scale range (mm^3) is one of the advantages of OCT compared with other imaging techniques.

Obtaining 3D biomass structures formed under representative conditions for spiral wound membrane systems may be used as additional tool to better understand the impact of different operational conditions on the biomass formation and to evaluate the effect of control strategies on the biomass structure. *In-situ* real time detailed image analysis on the acquired biomass morphology could be used to evaluate how the biomass structure responds to the operational conditions (*i.e.* feed pressure).

The proposed approach for analyzing OCT scans can be used to evaluate biomass development: (i) under various operating conditions, (ii) on different membranes and spacers (e.g. coatings/modifications) and (iii) in the presence of biocides.

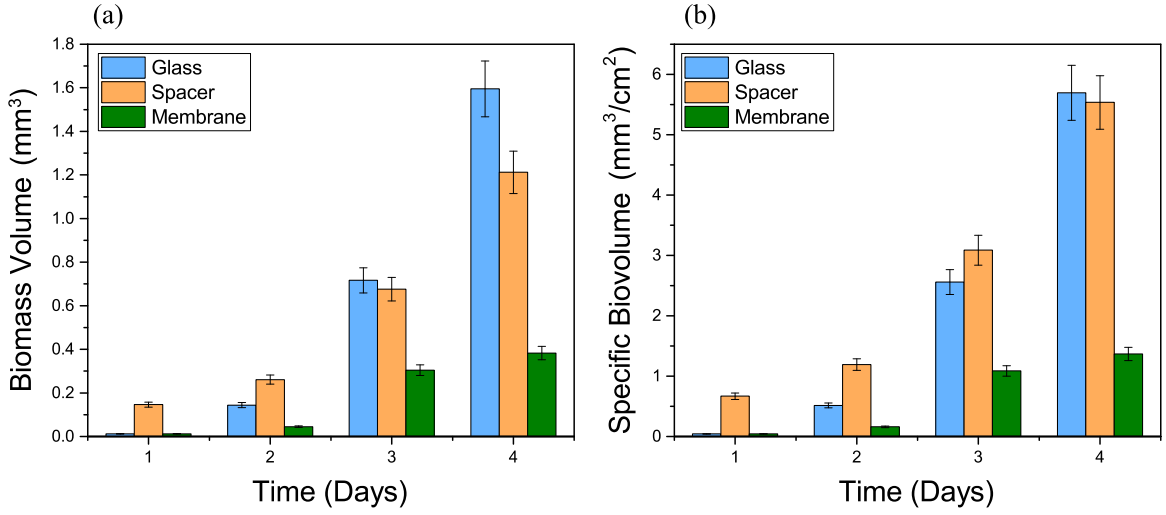

Fig. 7. Biomass volume (a) and specific biovolume (b) in time on the feed spacer, and membrane surface in the MFS. Specific biovolume is the biomass volume over the available surface area (area of both membrane and cover glass was each 28 mm^2 and of feed spacer was 21.9 mm^2).

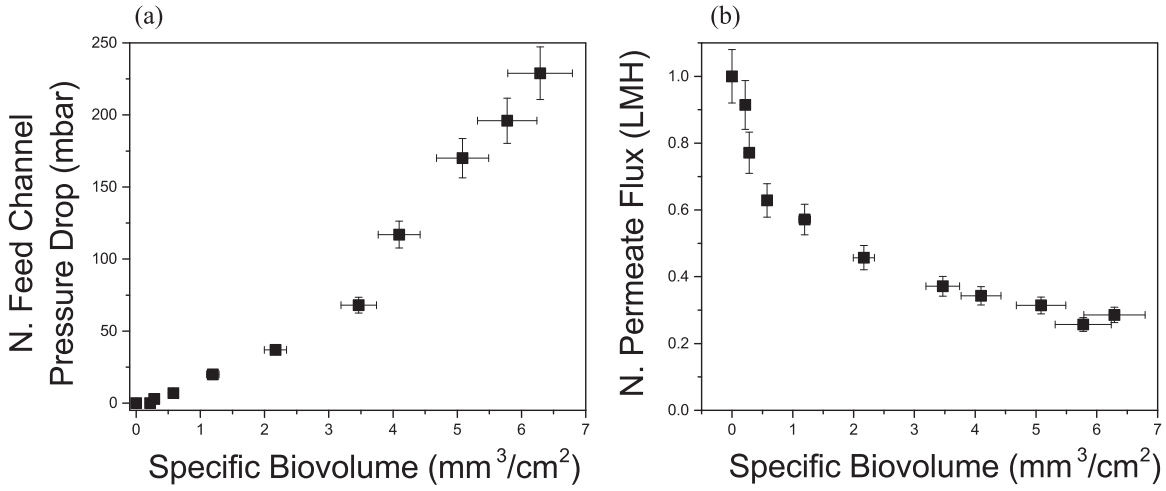

Fig. 8. Normalized feed channel pressure drop (a), and permeate flux (b) as function of the accumulated biovolume during the 5 day experimental period.

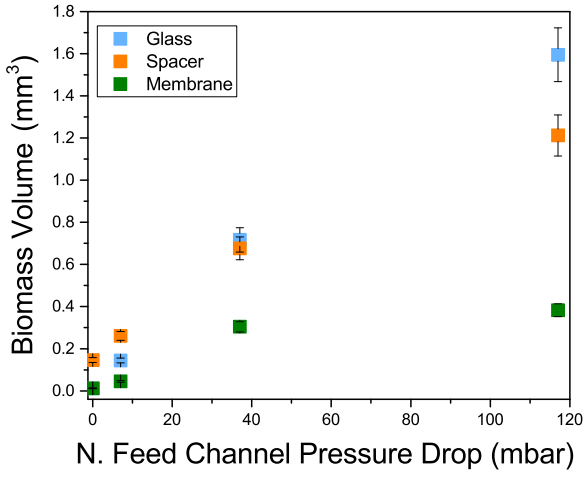

Fig. 9. Accumulated biomass volume on the three different elements (membrane, feed spacer and cover glass) in function of feed channel pressure drop increase.

phase the biofilm is a thin porous structure with low hydraulic resistance, meaning that the membrane surface coverage will be the main factor which impacts water flux [19]. As the biofilm grows (*i.e.* more biomass volume), thickness, porosity and hydraulic resistance change. Studies have shown that young biofilms are less porous and tend to have a low hydraulic resistance compared to a mature biofilm [29,31]. The rapid flux decline observed in the early stage of biomass accumulation may be attributed to the pore blocking fouling mechanism in UF membranes [32]. Once the biomass layer is formed on the membrane surface the flux depends mainly on its properties and the flux decline rate decreases (Fig. 6c, days 3 and 4). As shown in Fig. 7a, on the third and fourth day the biomass volume only slightly increases on the membrane surface while sharply increases on the other two elements (feed spacer and glass).

The biomass accumulation in the flow channel had different impact on the membrane performance parameters. While the pressure drop increases as the biomass increases, the permeate flux decrease is significantly affected in the initial phase of biomass accumulation.

4.2. Biomass accumulation and membrane performance

The delay in increasing feed channel pressure drop with respect to the biomass increase as detected by OCT scans can be explained by the higher sensitivity of the OCT and the position of the scanned area. When biofilm starts to form and grow in the feed channel the pressure drop starts to increase. However, in an early stage of biomass accumulation the biomass may not have an immediate impact on feed channel pressure drop. Bucs et al. [28] demonstrated that a 5 μm thin biofilm and small biofilm patches in the flow channel might not be detected by feed channel pressure drop measurements. Conversely, OCT imaging allows to capture and visualize these thin biofilms.

The higher impact on feed channel pressure drop increase of biomass accumulation on the feed spacer has been observed in other studies as well [28]. As shown in Fig. 9 the biomass accumulated on the membrane has lower impact on the feed channel pressure drop in respect to the biomass accumulated on the other elements.

The effect of biomass on permeate flux in spiral wound elements (reverse osmosis, nanofiltration) depends on the membrane surface coverage, flow channeling, biofilm hydraulic resistance, biofilm porosity and thickness [29]. At the initial phase of biofilm formation, studies showed that a thin biofilm layer is deposited on the surface [30]. At this

4.3. Biomass location in the flow channel

The biomass accumulation occurred mainly on the feed spacer in the early stages may be an indication of either a higher affinity of bacteria to attach to the feed spacer material (polypropylene) or preferential deposition due to the hydrodynamics of the system. Other studies have also reported that at initial stages of biomass formation, more biomass accumulates on the feed spacer than on the membrane surface [2,33,34]. As reported in Vrouwenvelder et al. [2] feed spacers play an important role in biofouling development and also in membrane cleanability [35].

A lower biomass volume was measured on the membrane surface compared to the cover glass surfaces (Fig. 7). The difference in the biomass volume distribution in flow cell can be attributed to the water flux through the membrane or the flow cell design. For this study a UF membrane was used, resulting in a high water flux (105 LMH). It was shown previously that the biomass compacts, decreasing in thickness and thus in biomass volume under high flux conditions [15,36]. This may have affected the measured biomass volume and underestimated the amount on the membrane surface. However, in a spiral wound membrane systems the flow channel is delimited by membranes on both sides therefore the biomass accumulated on the membrane surface may have a lower impact on the feed channel pressure drop.

4.4. Use of OCT in biofouling studies

The main advantage of OCT is that it allows observation and monitoring of biomass development during MFS operation without sample preparation such as the use of stains or contrast agents.

The effect of various cleaning strategies (e.g. chemical cleaning, air flushing, back washing *etc.*) on biomass developed can also be evaluated. Moreover, the reconstructed 3D biomass structures can be further imported into modeling software for mathematical modeling to increase the understanding of biofouling processes. The 3D biomass analysis presented in this study shows that OCT is a promising tool to study biofouling in membrane systems.

5. Conclusions

The experimental evaluation of biomass development in the membrane fouling simulator operated with permeate production using 3D reconstructed OCT scans leads to the following conclusions:

- The applied imaging approach consisting of subtracting the scan at time zero to the subsequent scans is suitable for evaluation of biofilm development. It enables spatial quantification of biofilm in a flow channel with feed spacer and membrane and also eliminates the signals due to other elements and reduces the background noise of the raw images.
- OCT detects biofouling before membrane performance is affected. The presence of biomass was confirmed by OCT one day earlier than performance decline was observed with the used setup.
- Early stage biofouling occurs mainly on the feed spacer. Analysis of the biomass accumulation showed a higher biomass volume on the feed spacer than on the membrane surface. Also the feed channel pressure drop was mainly affected by the biomass accumulated on the feed spacer.
- Accumulated biomass differs in impact on feed channel pressure drop increase and flux decrease. Feed channel pressure drop continuously increased with biomass volume increasing, while the permeate flux was mainly affected in the initial phase of biomass accumulation.

Acknowledgement

This study was supported by funding from King Abdullah University of Science and Technology (KAUST).

Appendix A. Supplementary material

Supplementary data associated with this article can be found in the online version at doi:10.1016/j.memsci.2016.11.052.

References

[1] H.F. Ridgway, H.-C. Flemming, Membrane biofouling in water treatment membrane processes, Water Treat. Membr. Process. (1996).
[2] J.S. Vrouwenvelder, S.A. Manolarakis, J.P. van der Hoek, J.A.M. van Paassen, W.G.J. van der Meer, J.M.C. van Agtmaal, et al., Quantitative biofouling diagnosis in full scale nanofiltration and reverse osmosis installations, Water Res. 42 (2008) 4856–4868. http://dx.doi.org/10.1016/j.watres.2008.09.002.
[3] A. Matin, Z. Khan, S.M.J. Zaidi, M.C. Boyce, Biofouling in reverse osmosis membranes for seawater desalination: Phenomena and prevention 281 (2011) 1–16. http://dx.doi.org/10.1016/j.desal.2011.06.063.
[4] H. Hemming, A. Tamachkiarowa, J. Klahre, J. Schmitt, Monitoring of fouling and biofouling in technical systems, Water Sci. Technol. 38 (1998) 291–298. http://dx.doi.org/10.1016/S0273-1223(98)00704-5.
[5] H.C. Flemming, Role and levels of real-time monitoring for successful anti-fouling strategies - An overview inWater Sci. Technol. (2003) 1–8 ⟨http://www.scopus.com/inward/record.url?eid=2-s2.0-0037268213&partnerID=tZOtx3y1⟩.
[6] J. Vrouwenvelder, J. Van Paassen, L. Wessels, A. Van Dam, S. Bakker, The Membrane Fouling Simulator: A practical tool for fouling prediction and control, J. Memb. Sci. 281 (2006) 316–324. http://dx.doi.org/10.1016/j.memsci.2006.03.046.
[7] B. Halan, K. Buehler, A. Schmid, Biofilms as living catalysts in continuous chemical syntheses, Trends Biotechnol. 30 (2012) 453–465. http://dx.doi.org/10.1016/j.tibtech.2012.05.003.
[8] M. Herzberg, M. Elimelech, Biofouling of reverse osmosis membranes: Role of biofilm-enhanced osmotic pressure, J. Memb. Sci. 295 (2007) 11–20. http://dx.doi.org/10.1016/j.memsci.2007.02.024.
[9] H.-C. Flemming, J. Wingender, The biofilm matrix, Nat. Rev. Micro. 8 (2010) 623–633.
[10] R. Valladares Linares, L. Fortunato, N.M. Farhat, S.S. Bucs, M. Staal, E.O. Fridjonsson, et al., Mini-review: novel non-destructive in situ biofilm characterization techniques in membrane systems, Desalin. Water Treat. (2016) 1–8. http://dx.doi.org/10.1080/19443994.2016.1180483.
[11] N. Derlon, M. Peter-Varbanets, A. Scheidegger, W. Pronk, E. Morgenroth, Predation influences the structure of biofilm developed on ultrafiltration membranes, Water Res. 46 (2012) 3323–3333. http://dx.doi.org/10.1016/j.watres.2012.03.031.
[12] Y. Wibisono, K.E. El Obied, E.R. Cornelissen, a. J.B. Kemperman, K. Nijmeijer, Biofouling removal in spiral-wound nanofiltration elements using two-phase flow cleaning, J. Memb. Sci. 475 (2015) 131–146. http://dx.doi.org/10.1016/j.memsci.2014.10.016.
[13] N. Derlon, N. Koch, B. Eugster, T. Posch, J. Pernthaler, W. Pronk, et al., Activity of metazoa governs biofilm structure formation and enhances permeate flux during Gravity-Driven Membrane (GDM) filtration, Water Res. 47 (2013) 2085–2095. http://dx.doi.org/10.1016/j.watres.2013.01.033.
[14] L. Fortunato, S. Jeong, Y. Wang, A.R. Behzad, T. Leiknes, Integrated approach to characterize fouling on a flat sheet membrane gravity driven submerged membrane bioreactor, Bioresour. Technol. 222 (2016) 335–343. http://dx.doi.org/10.1016/j.biortech.2016.09.127.
[15] C. Dreszer, A.D. Wexler, S. Drusová, T. Overdijk, A. Zwijnenburg, H.-C. Flemming, et al., In-situ biofilm characterization in membrane systems using Optical Coherence Tomography: formation, structure, detachment and impact of flux change, Water Res. 67 (2014) 243–254. http://dx.doi.org/10.1016/j.watres.2014.09.006.
[16] F. Blauert, H. Horn, M. Wagner, Time-resolved biofilm deformation measurements using optical coherence tomography, Biotechnol. Bioeng. 112 (2015) 1893–1905. http://dx.doi.org/10.1002/bit.25590.
[17] L. Fortunato, A. Qamar, Y. Wang, S. Jeong, T. Leiknes, In-situ assessment of biofilm formation in submerged membrane system using optical coherence tomography and computational fluid dynamics, J. Memb. Sci. 521 (2017) 84–94. http://dx.doi.org/10.1016/j.memsci.2016.09.004.
[18] X. Yang, H. Beyenal, G. Harkin, Z. Lewandowski, Quantifying biofilm structure using image analysis, J. Microbiol. Methods. 39 (2000) 109–119. http://dx.doi.org/10.1016/S0167-7012(99)00097-4.
[19] S. West, M. Wagner, C. Engelke, H. Horn, Optical coherence tomography for the in situ three-dimensional visualization and quantification of feed spacer channel fouling in reverse osmosis membrane modules, J. Memb. Sci. 498 (2015) 345–352. http://dx.doi.org/10.1016/j.memsci.2015.09.047.
[20] C. Li, S. Felz, M. Wagner, S. Lackner, H. Horn, Investigating biofilm structure developing on carriers from lab-scale moving bed biofilm reactors based on light microscopy and optical coherence tomography, Bioresour. Technol. 200 (2016) 128–136. http://dx.doi.org/10.1016/j.biortech.2015.10.013.
[21] J.S. Vrouwenvelder, S.M. Bakker, L.P. Wessels, J.A.M. van Paassen, The Membrane Fouling Simulator as a new tool for biofouling control of spiral-wound membranes, Desalination 204 (2007) 170–174. http://dx.doi.org/10.1016/j.desal.2006.04.028.
[22] J.S. Vrouwenvelder, C. Hinrichs, W.G.J. Van der Meer, M.C.M. Van Loosdrecht, J.C. Kruithof, Pressure drop increase by biofilm accumulation in spiral wound RO and NF membrane systems: role of substrate concentration, flow velocity, substrate load and flow direction, Biofouling 25 (2009) 543–555. http://dx.doi.org/10.1080/08927010902972225.
[23] S.S. Bucs, N. Farhat, A. Siddiqui, R. Valladares Linares, A. Radu, J.C. Kruithof, et al., Development of a setup to enable stable and accurate flow conditions for membrane biofouling studies, Desalin. Water Treat. 57 (2015) 12893–12901. http://dx.doi.org/10.1080/19443994.2015.1057037.
[24] N. Otsu, Threshold selection method from gray-level histograms, IEEE Trans. Syst. Man. Cybern. SMC 9 (1979) 62–66 ⟨http://www.scopus.com/inward/record.url?eid=2-s2.0-0018306059&partnerID=tZOtx3y1⟩.
[25] M. Wagner, D. Taherzadeh, C. Haisch, H. Horn, Investigation of the mesoscale structure and volumetric features of biofilms using optical coherence tomography, Biotechnol. Bioeng. 107 (2010) 844–853. http://dx.doi.org/10.1002/bit.22864.
[26] A.I. Radu, M.S.H. van Steen, J.S. Vrouwenvelder, M.C.M. van Loosdrecht, C. Picioreanu, Spacer geometry and particle deposition in spiral wound membrane feed channels, Water Res. 64 (2014) 160–176. http://dx.doi.org/10.1016/j.watres.2014.06.040.
[27] S.S. Bucs, R.V. Linares, J.O. Marston, A.I. Radu, J.S. Vrouwenvelder, C. Picioreanu, Experimental and numerical characterization of the water flow in spacer-filled channels of spiral-wound membranes, Water Res. 87 (2015) 299–310. http://dx.doi.org/10.1016/j.watres.2015.09.036.
[28] S.S. Bucs, A.I. Radu, V. Lavric, J.S. Vrouwenvelder, C. Picioreanu, Effect of different commercial feed spacers on biofouling of reverse osmosis membrane systems: A numerical study, Desalination. 343 (2014) 26–37. http://dx.doi.org/10.1016/j.desal.2013.11.007.
[29] C. Dreszer, J.S. Vrouwenvelder, A.H. Paulitsch-Fuchs, A. Zwijnenburg, J.C. Kruithof, H.C. Flemming, Hydraulic resistance of biofilms, J. Memb. Sci. 429 (2013) 436–447. http://dx.doi.org/10.1016/j.memsci.2012.11.030.
[30] H.-C. Flemming, G. Schaule, T. Griebe, J. Schmitt, A. Tamachkiarowa, Biofouling—the Achilles heel of membrane processes, Desalination. 113 (1997) 215–225.

http://dx.doi.org/10.1016/S0011-9164(97)00132-X.
[31] K.J. Martin, D. Bolster, N. Derlon, E. Morgenroth, R. Nerenberg, Effect of fouling layer spatial distribution on permeate flux: A theoretical and experimental study, J. Memb. Sci. 471 (2014) 130–137. http://dx.doi.org/10.1016/j.memsci.2014.07.045.
[32] F. Wang, V.V. Tarabara, Pore blocking mechanisms during early stages of membrane fouling by colloids, J. Colloid Interface Sci. 328 (2008) 464–469. http://dx.doi.org/10.1016/j.jcis.2008.09.028.
[33] J. Baker, T. Stephenson, S. Dard, P. Cote, Characterisation of fouling of nanofiltration membranes used to treat surface waters, Environ. Technol. 16 (1995) 977–985 ⟨http://www.scopus.com/inward/record.url?eid=2-s2.0-0029616603&partnerID=tZOtx3y1⟩.
[34] J.A.M. Van Paassen, J.C. Kruithof, S.M. Bakker, F.S. Kegel, Integrated multi-objective membrane systems for surface water treatment: pre-treatment of nanofiltration by riverbank filtration and conventional ground water treatment, Desalination. 118 (1998) 239–248. http://dx.doi.org/10.1016/S0011-9164(98)00137-4.
[35] S.A. Creber, J.S. Vrouwenvelder, M.C.M. van Loosdrecht, M.L. Johns, Chemical cleaning of biofouling in reverse osmosis membranes evaluated using magnetic resonance imaging, J. Memb. Sci. 362 (2010) 202–210. http://dx.doi.org/10.1016/j.memsci.2010.06.052.
[36] R. Valladares Linares, A.D. Wexler, S.S. Bucs, C. Dreszer, A. Zwijnenburg, H.-C. Flemming, et al., Compaction and relaxation of biofilms, Desalin, Water Treat. (2015) 1–13. http://dx.doi.org/10.1080/19443994.2015.1057036.